Sasikala et al. Sustainable Environment Research (2019) 29:1
https://doi.org/10.1186/s42834-019-0001-z

Sustainable Environment Research

RESEARCH Open Access

Competitive photo-degradation performance of ZnO modified bentonite clay in water containing both organic and inorganic contaminants

Suchithra Padmajan Sasikala[1,2*], T. A. Nibila[1], Kunnathuparambil Babu Babitha[1], Abdul Azeez Peer Mohamed[1] and Ananthakumar Solaiappan[1*]

Abstract

This study reports the activity difference of zinc oxide modified bentonite clay (Photo-Zn-Bent) photocatalyst when in contact with different environmentally toxic pollutants in a single component and bi-component pollutant systems. The layered structure of purified and swollen nano-bentonite clay (Bent) has tunable interlayer spacing to grow zinc oxide (ZnO) nanoparticles, thereby integrating the adsorbing nature of clay and semiconductor property of ZnO in one hierarchical structure. Initial adsorption studies using methylene blue (MB) showed that the adsorption capacity of Photo-Zn Bent is greater than Bent and ZnO. The photocatalytic pollutant degradation activity of Photo-Zn Bent is compared with ZnO using both single component and bi-component pollutant systems (MB, phenol, mixture of MB and phenol, mixture of phenol and Cr(VI)). We found that Photo-Zn Bent displayed 33% greater MB degradation rate compared to ZnO. Photodegradation efficiency of Photo-Zn-Bent considerably differs for inorganic-organic and organic-organic bicomponent pollutant systems. In bicomponent systems, photodegradation rate of phenol decreased to an extent of 88% in the presence of MB, and increased to 31% in the presence of Cr(VI). On the other hand, photodegradation rate of MB remains unaffected in the presence of phenol, but increased to 56% in the presence of Cr(VI). However, if used in bicomponent pollutant systems for simultaneous cycles, Photo-Zn Bent showed lesser activity after 3 cycles, which in turn gave further insight on to the decay of catalyst with respect to the nature of pollutants.

Keywords: ZnO, Bentonite, Chromium(VI), Dye, Phenol, Photodegradation

Introduction

Among environmentally harmful organic contaminants, phenols and dyes are primary toxic contaminants which are detrimental even at ppb levels to the aquatic/human life [1, 2]. Similarly, hexavalent chromium [Cr(VI)] is a toxic inorganic industrial pollutant. The toxicity of chromium is associated to its oxidation state. Thus Cr(VI) is carcinogenic to living organisms including humans, whereas trivalent state of chromium [Cr(III)] is nontoxic [3, 4]. Industries such as petroleum refining, fiberboard, coal mine, chemical, dye, textile pulp mill, paint, and steel dispose of Cr(VI) together with phenols and dyes through their effluents [5, 6]. Degradation of these combinations of pollutants is not an easy task without stronger oxidizing agents ($KMnO_4/H_2O_2$). However, using those oxidizing agents is considered as environmentally unfriendly because the reactant and end products from the redox reaction are also pollutants [7]. Adsorption and very recently photocatalysis have emerged as economically and technically attractive methods for various water purification and recycling processes. Development of low-cost adsorbents based on natural clays such as zeolite and bentonite for removing soluble organics from wastewater is a hot research topic as evident from the increasing number of publications every year [8–12].

* Correspondence: schithraps@gmail.com; ananthakumar70@gmail.com
[1]Functional Materials, Materials Science and Technology Division, National Institute for Interdisciplinary Science and Technology, Trivandrum 695 019, India
[2]Department of Material Science and Engineering, Korea Advanced Institute of Science and Technology, Daejeon 34141, Republic of Korea

The main reason for this selection is the susceptibility of layered clays to organic/inorganic modifications apart from their large internal surface area. But adsorption simply transfer contaminants from one phase to another which demands further chemical treatment for the recovery of the adsorbent material [13, 14]. Also, excessive usage of adsorbents gradually leads to problems with landfill. In this scenario photocatalytic degradation of organic contaminants without leaving any traces of secondary pollutants is even more significant [15].

Among many metal oxides and sulfides scrutinized as photocatalyst for photodegradation of organics from aqueous solution, ZnO is interesting due to its non-toxic nature, comparatively high photocatalytic ability, chemical and thermal stability and synthesis feasibility [9, 16]. But instability of ZnO in acidic conditions, photo-corrosive nature and spontaneous growth and aggregation restrict its applicability in wastewater treatment [17, 18]. In order to overcome this, a methodology commonly practiced is to incorporate ZnO into suitable porous inorganic matrix like activated carbon, zeolites, MCM-41, clay and silica [1, 19–21]. In addition, these matrixes help concentrate pollutants by adsorption into the vicinity of ZnO for simultaneous photo degradation.

Nevertheless, the previously reported clay/carbon based photocatalytic materials are analysed for their photo degradation behaviour of individual organic pollutants (mostly dyes) [22–25]. However, it is more likely that industrial wastewaters contain both organic and inorganic contaminants. As mentioned before the effluents from common industries such as textile, paint and steel contain a combination of pollutants such as dyes, phenol and Cr(VI) together with traces of heavy metals. The cohabitation of contaminants hinders the degradation rate due to the competition between contaminants and the reaction intermediates generated during the course of photodegradation for the limited number of active sites on the catalyst surface [12, 26]. It is expected that well dispersion of photocatalytic nanoparticles over porous media enables to construct more active surface. The porous media help in concentrating the pollutants into the catalyst surface. The increased contact between pollutants and catalyst sites promotes better photodegradation performance.

In addition, studies relating to the effect of nature of contaminants on photoactivity and catalyst lifetime shall be important for its real-life application which is scarcely investigated in the past to the best of our information. Thus, the core objective of this work is to investigate the behaviour of ZnO/clay hybrid (Photo-Zn-Bent) in single component and bi-component systems in which both organic and inorganic pollutants co-exist. We have also investigated the recyclability difference of Photo-Zn-Bent in different single and bi-component pollutant systems.

Materials and methods

Materials

Zinc acetate ($Zn(Ac)_2 \cdot 2H_2O$, 99.9%, E-Merck), poly vinyl alcohol (PVA, E-Merck), potassium dichromate ($K_2Cr_2O_7$, 99.9%, SDFCL), ethanol (C_2H_5OH), methylene blue (MB, $C_{16}H_{18}N_3SC_l$), phenol (C_6H_5OH), 1,5-diphenyl carbazide, sulphuric acid (H_2SO_4, 98%), were used as received. Indian origin clay mineral (bentonite) was obtained from Central Drug House Pvt. Ltd., Mumbai. Stock solution of contaminants (Cr(VI), MB and phenol) contain 1 g each of $K_2Cr_2O_7$, MB and phenol in 1000 mL of deionised water. Working standard solution of contaminants was the required aqueous dilutions of stock solution.

Synthesis of nano-bentonite clay (Bent)

Raw clay may contain many impurities, so extensive purification procedure was needed to purify the clay particles for the present study. A clay suspension (5 g bentonite clay in 1 L deionized water) was stirred for 24 h, and subsequently separated after discarding the sediments before centrifugation at 7000 rpm for 1 h. The sedimented clay was collected and repeatedly carried out the suspension and centrifugation as described above for at least 5 times. 10 g of the bentonite obtained from the above described purification procedure is suspended in 1 L of 1.0 M NaCl solution for 12 h to exchange interlayer cations in bentonite clay with Na^+. The ion exchanged bentonite is collected by centrifugation and rinsed with deionized water several times to remove chlorine ions (until the filtrate show no white colour in 10% silver nitrate solution) and dried at 80 °C. 10 g of as obtained sodium exchanged clay (Na^+-Bent) suspended in 250 mL deionized water until a homogenous suspension is achieved with the help of ultrasonication. The suspension is then centrifuged at 5000 rpm and the top portion is recovered, dried and ground to get Bent.

Sol-gel route to nanocatalyst (Photo-Zn-Bent) and ZnO

Process flow chart for synthesis of Photo-Zn-Bent is shown as Scheme S1 in Supplementary Material. The precursor used for the synthesis of ZnO in the present study was Zinc acetate ($Zn(Ac)_2 \cdot 2H_2O$. In a typical synthesis, 1.5 g $Zn(Ac)_2 \cdot 2H_2O$ was suspended in 50 mL ethanol:water (3:1) mixture by constant stirring. 0.5 g of PVA solution was added to the mixture drop wise and stirred until a homogenous sol is obtained. To this 0.05 g of Na-bentonite swelled by the aid of ultrasonication (for 30 min) in distilled water is added drop wise with vigorous stirring and continued to stir for 1 h for effective intercalation of Zn precursor inside the clay layers, before increasing the temperature of the resulted sol to 70 °C. After 30 min vigorous stirring, the temperature of the sol increased to 120 °C and the

reaction vessel was kept open for slow evaporation of the solvent. A yellow tinted viscous thick gel formed was washed with deionised water to remove the surface adsorbed PVA, dried and calcined at 600 °C for 4 h. The resulted catalyst (Photo-Zn-Bent) was finely ground and sieved and kept in desiccators for further analysis. The same procedure repeated without adding Bent to obtain ZnO for comparative studies.

Characterization of materials

Crystal structure of Bent, ZnO and Photo-Zn-Bent was analysed by powder X-ray diffraction using Philips X-ray diffractometer (X'Pert Pro, Cu Kα radiation, $\lambda = 0.154$ nm), while thermo gravimetric analysis (TGA) was carried out using Mettler TG 50 (Shimadzu, Kyoto). Morphology analysis of the samples was carried out using JEOL 5600 SL scanning electron microscope (SEM) and JEOL 200 CX transmission electron microscope (TEM). Elemental analysis of the samples was carried out by energy-dispersive X-ray spectroscopy (EDS) using EDX model-INCA oxford. Surface area and porosity of the samples were determined by the Brunauer-Emmet-Teller (BET) technique using a Micromeritics Gemini 2370 instrument that used a N_2/77 K adsorption-desorption method. A UV-Visible spectrophotometer (Jasco model V-530) was used for the determination of concentration MB, phenol and Cr(VI) in aqueous solution. Atomic absorption spectrometry (AAS) analysis was used to determine the total Cr ion concentration before and after the photocatalytic experiments. Cary Eclipse was used for the spectrophotometric analysis of the powder samples. Photon Correlation Spectroscopic analysis was performed using Malvern Zeta Sizer.

Adsorption and photocatalysis experiments

The photocatalytic degradation occurs predominantly on the surface of photocatalyst. Thus, initial adsorption of pollutant ions from aqueous solution onto photocatalyst surface is an important reaction which needs to be well investigated. Therefore, our initial focus was to determine the extent of adsorption of the pollutant to the catalyst surface. In a typical adsorption experiment, 0.1 g catalyst is stirred with 50 mL of pollutant (adsorbent dose 2 g L^{-1}) in dark atmosphere. The dark atmosphere was created by sealing the reaction bottles with silver foil and stirred using a magnetic stirrer placed in a closed box to avoid sunlight. The adsorption experiments were conducted using different initial pollutant concentration (10 to 250 mg L^{-1}) and different adsorption duration (5 min up to 2 h). Photocatalysis experiments were done after evaluating optimum conditions for adsorptions equilibrium. Once adsorption equilibrium is attained, aluminium foil covering the reaction vessel was discarded and the reaction vessel was transferred for photocatalysis experiments. For the photocatalysis experiments, the reaction was allowed to progress under constant stirring for another 4 to 5 h inside a photoreactor (Rayonet) containing 15 W tubes (Philips G15 T8) as the UV-source, which emitted the UV-radiation having wavelength within the range of 200–400 nm (corresponding to the photon energy range of 3.07–6.14 eV).

Both adsorptive and photocatalytic removal rate of pollutants was monitored by measuring the absorbance of the aliquot solution using the UV-Vis spectrophotometer. We have analysed each pollutant systems before and after adsorption/photocatalysis experiment. The major absorption band of MB and phenol was around 656 and 270 nm, respectively. Cr(VI) concentration was estimated spectrophotometrically using the conventional colorimetric method by measuring the purple complex of Cr(V1) with 1,5-diphenylcarbazide at 540 nm against a reagent blank in UV-Vis spectrophotometer. Note that, the absorption peak can be raised from the presence of photodegradation intermediates, also disappearance of characteristic absorption peak denotes complete elimination of respective pollutants and their intermediates from the tested solution. A maximum of 5 replicates were performed for each experiment. All experimental points in the reported isotherm/kinetic plots fall in ± 5% error bar.

Results and discussion

Synthesis and characterization

The present work realized in situ pillaring of nano ZnO in between aluminosilicate clay layers to generate a hybrid with discrete and uniformly distributed photoactive sites on a matrix with wider surface area (Fig. 1a). We used zinc acetate as precursor for ZnO, since acetates (Ac) are good complexing ligands for Zn(II) as described by following equations [27].

$$Zn - OAc + HOH/OH^- \leftrightarrow Zn - OH + (HOAc/AcO^-) \quad (1)$$

$$Zn - OH + Zn - OAc \leftrightarrow Zn - O - Zn + HOAc \quad (2)$$

$$Zn - OH + Zn - OAc \leftrightarrow Zn - O - Zn + HOAc \quad (3)$$

$$Zn - OH \xrightarrow{\Delta} ZnO \quad (4)$$

Figure 1b shows the TGA curves of Bent, Zn(Ac)/Bent (before calcination to form Photo-Zn-Bent), ZnO and Photo-Zn-Bent. TGA of Bent displayed two-stage decomposition: (i) about 7.3% weight loss at 80–120 °C due to the evaporation of absorbed moisture and (ii) 5.3% weight loss at 120–500 °C due to the loss of interlayer water and structural OH groups [28]. The TG

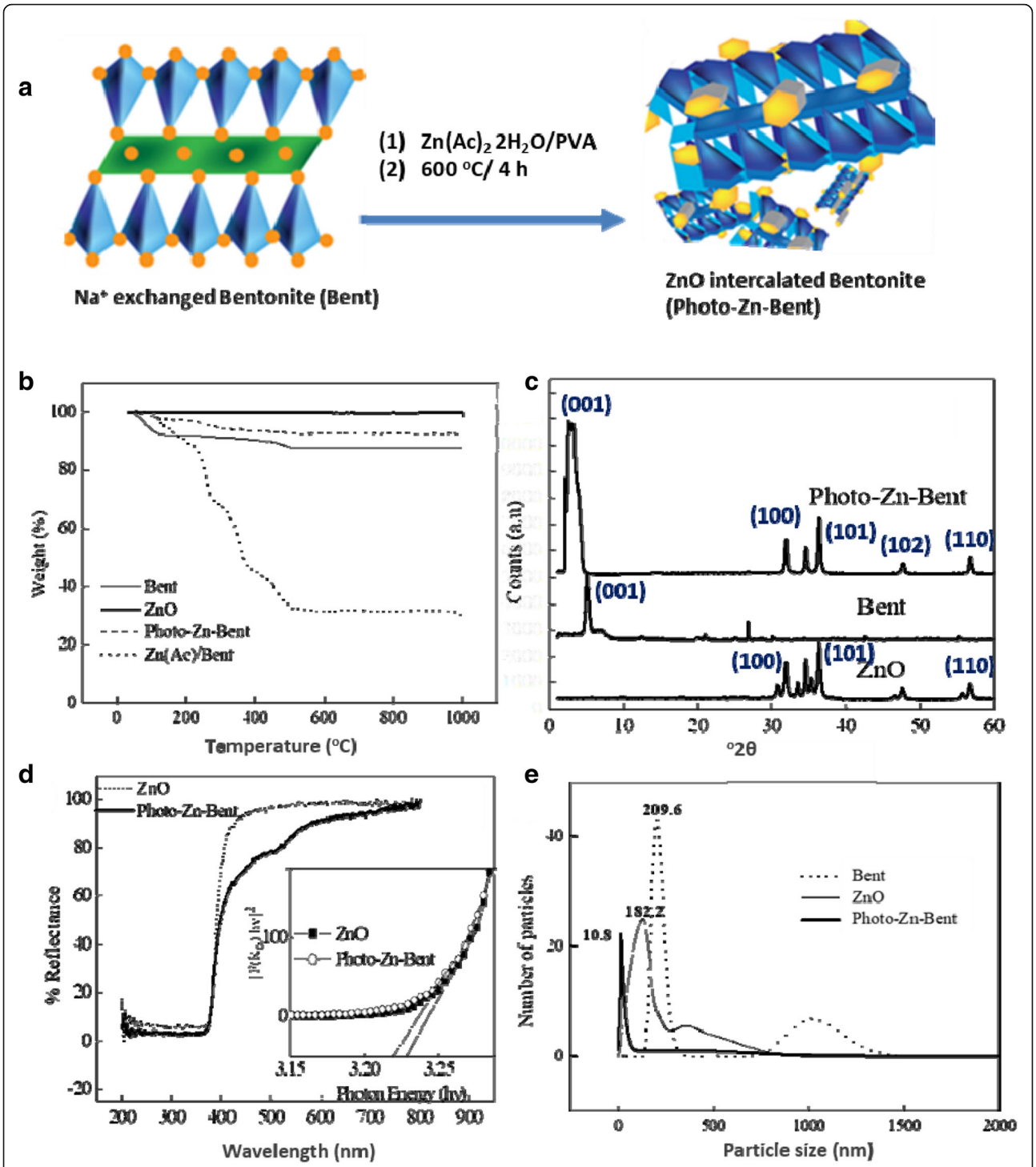

Fig. 1 (**a**) Schematic representation of synthesis of Photo-Zn-Bent, (**b**) TGA pattern of Bent, Zn(Ac)/Bent, ZnO and Photo-Zn-Bent, (**c**) XRD pattern of ZnO, Bent and Photo-Zn-Bent, (**d**) DRS spectra of ZnO and Photo-Zn-Bent. Inset of (**d**) shows Kubelka-Munk transformed reflectance spectra of ZnO and Photo-Zn-Bent. (**e**) Photon correlation spectra of Bent, ZnO and Photo-Zn-Bent showing particle size distribution

curve of as prepared Zn(Ac)/Bent showed a drastic weight loss of 68.1% up to 500 °C comprising different consecutive decomposition stages. The first weight loss (~10.4%) up to 200 °C may be related to the loss of absorbed moisture together with dehydration of zinc acetate to form anhydrous zinc acetate. Around 57.7% of initial weight was lost between 200 to 500 °C. The TGA curve showed three successive decomposition stages,

implying that the PVA polymeric network used for capping was slowly burnt through the outer surface and zinc acetate salt was calcinated and converted into ZnO. This agrees with other literature citing that thermal decomposition of PVA begin at about 230 °C and continue up to 480 °C until complete decomposition on the side and main chains of PVA [29]. Wang et al., reported that the decomposition of anhydrous zinc acetate occurred from about 245 to 312 °C caused growth of ZnO [30]. There was no apparent weight loss above 500 °C, indicating the formation of pure ZnO. It was in accordance with TG curve of ZnO, which was calcined at 500 °C and showed absence of any trace of thermal decomposition in the entire temperature region. But TGA of Photo-Zn-Bent showed about 5.5% weight loss in the region 100–500 °C related to the loss of absorbed moisture and dehydroxylation of aluminosilicate layers. However, compared to precursor Bent, Photo-Zn-Bent showed enhanced thermal stability, implying that ZnO had been exchanged with interlayer water molecules of Bent, which was further confirmed by XRD results obtained for ZnO, Bent and Photo-Zn-Bent (Fig. 1c).

The diffraction peaks at 2θ equalling to 31.91, 34.57, 36.39, 47.68 and 56.73° with d-spacing of 2.80, 2.59, 2.47, 1.90 and 1.62 Å, respectively, in the XRD pattern of ZnO and Photo-Zn-Bent revealed hexagonal zincite phase of ZnO and can be indexed to crystal planes (100), (002), (101), (102) and (110), respectively (JCPDS file number 750526). The diffraction peak with characteristic d-spacing of 4.43 Å in the XRD pattern of Bent indicated 2:1 layered structure. The high intensity peak at 2θ equalling to 5.07° in the (001) crystal plane with d-spacing of 17.41 Å is resulted from the interlayer distance (d) in the Bent. The d has increased to 36.53 Å in the XRD pattern of Photo-Zn-Bent. Hence, we can assume intercalation of ZnO nanoparticles of the size 1–2 nm in the interlayer of Bent. The diffuse *reflectance* (DR) spectra of ZnO and Photo-Zn-Bent is shown in Fig. 1d. As shown, for pure ZnO, considerable reduction in reflectance started at around 454 nm, but for Photo-Zn-Bent, the wavelength at which reduction started is not evident suggesting the formation of band tail due to the presence of silicate layers [31]. The inset of Fig. 1d presents DR spectra of the samples after Kubelka-Munk treatment [32]. The intersection between the linear fit and the photon energy axis gives the value to Eg, the energy gap. As shown upon hybridization with Bent, the Eg value of ZnO showed a very slight red shift from 3.23 to 3.22 eV indicating higher crystalline nature of Photo-Zn-Bent than ZnO.

Photon correlation spectra (PCS) based on dynamic light scattering technology was recorded to obtain the particle size distribution of Bent, ZnO and Photo-Zn-Bent as shown in Fig. 1e. Bent showed bi-modal particle distribution with one sharp peak centred on 209.6 nm with maximum number of particles and one peak with an insignificant number of particles in 800–1300 nm size range, with FWHM (full width at half maximum) at 1054.4 nm. The distribution curve of ZnO was unimodal with FWHM calculated to be 182.2 nm. Compared to ZnO, the range of particle size distribution drastically decreased to 10.8 nm for Photo-Zn-Bent while the frequency distribution indicated a normal unimodal distribution curve. Compared to ZnO, the range of particle size distribution drastically decreased to 10.8 nm for Photo-Zn-Bent while the frequency distribution indicated a unimodal distribution curve in contrast to the expected bi-modal distribution curve. It can be assumed that the Bent restricted the growth of ZnO crystals, which is evident from the SEM (Additional file 1: Figure S2) and TEM (Fig. 2) images. The TEM image of ZnO showed spherical shaped particles of average diameter of 100–200 nm. However, in the TEM image of Photo-Zn-Bent, ZnO nanoparticles of average diameter 2–10 nm were found well dispersed in the clay layer of maximum size 1–2 μm. The unimodal distribution curve with FWHM of 10.8 nm in PCS measurement for Photo-Zn Bent can be ascribed to partially aggregated ZnO nanoparticles. The absence of distribution peak representing large clay layers can be attributed to the high frequency of ZnO nanoparticles against limited number of clay layers in the test solution.

The diffused ring patterns with intermittent intense spots in selected area diffraction pattern (X-ray diffraction) given by the nanoparticles (Fig. 2b, d and f) indicate the presence of polycrystalline nanoparticles. Further BET surface area of ZnO, Bent and Photo-Zn-Bent were calculated by using N_2 adsorption/desorption isotherm as presented in Additional file 1: Figure S3. ZnO, Bent and Photo-Zn-Bent displayed BET surface area of 3.4, 22.9 and 24.8 $m^2 g^{-1}$. The slight decrease in the surface area of Bent after intercalation with ZnO may be due to the presence of ZnO causing blockage of surface pores to some extent, leading to decreased adsorption of N_2 gas. Nevertheless, all the samples showed a mesoporous pore distribution of 2–4 nm. EDS of the samples (Additional file 1: Figure S3) displayed atomic weight percentage ratio of zinc to Bent as 0.73:1.0.

Adsorption vs photocatalytic experiments

To confirm the individual role of Bent, ZnO and Photo-Zn-Bent in the photo degradation process, two sets of experiments were performed, taking MB as model organic pollutant. One set was performed with catalysts (0.1 g) under dark (adsorption condition) and other set was performed under UV light irradiation (photocatalytic condition). 50 mL of MB dye (50 mg L^{-1})

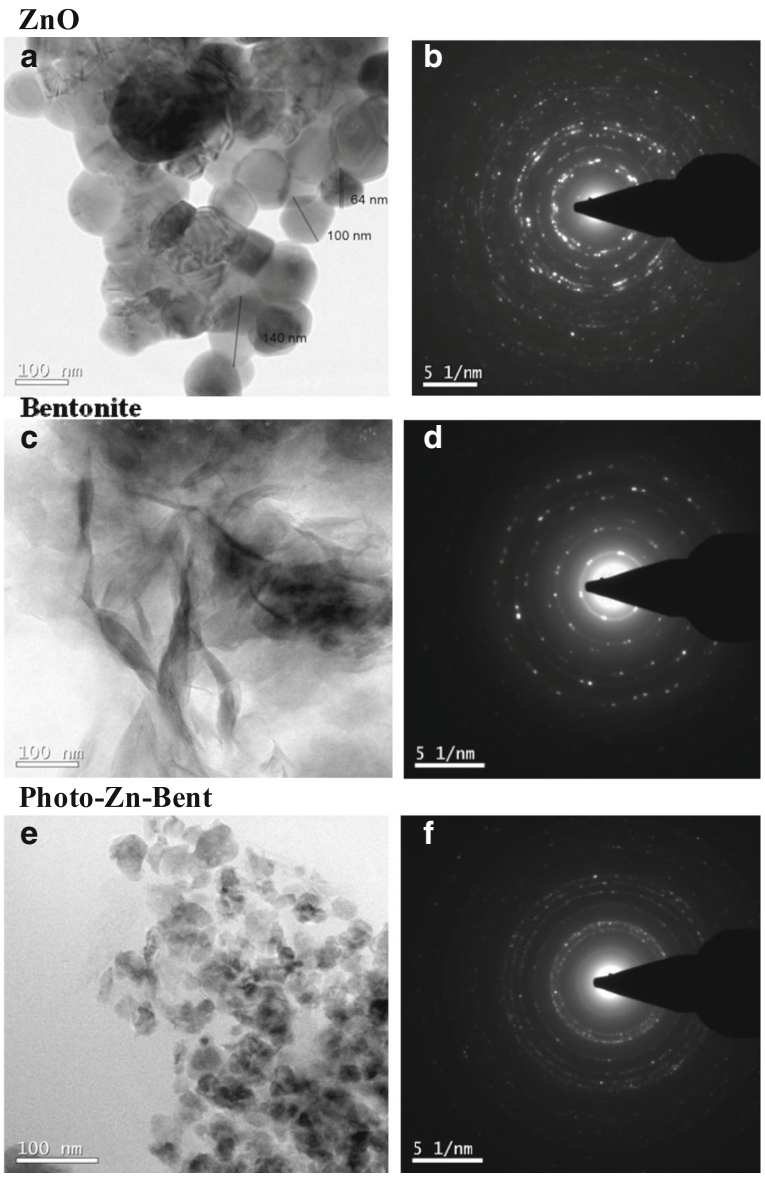

Fig. 2 High resolution transmission electron microscopy images (**a**, **c**, **e**) and selected area diffraction pattern (**b**, **d**, **f**) of samples. (**a**, **b**) ZnO, (**c**, **d**) Bent and (**e**, **f**) Photo-Zn-Bent

was selected as test solution. Adsorptive removal of MB followed the order: Bent > Photo-Zn-Bent > ZnO. ZnO could only remove about 2% of MB from aqueous solution, while Bent and Photo-Zn-Bent could remove 26 and 18%, respectively, by adsorption. This result was expected since BET surface area of Bent ($24.8\ m^2\ g^{-1}$) was decreased to $22.9\ m^2\ g^{-1}$ when combined with ZnO ($3.41\ m^2\ g^{-1}$). Upon UV irradiation, about 95% of initial MB was degraded from test solution exposed to Photo-Zn-Bent, while ZnO could degrade about 63%.

As expected, there were no detectable MB degradation in contact with Bent under UV light, and ZnO under dark atmosphere. The results are presented in Fig. 3a. As shown, Photo-Zn-Bent is much more effective for the removal of MB than independently. Localizing contaminants into the active catalyst sites can in fact improve the photo degradation rate. Therefore, adsorptive property of Photo-Zn-Bent is important in its photocatalytic efficiency. Combination of Bent of high surface area helps in the increase of adsorbed pollutant concentration on ZnO surface.

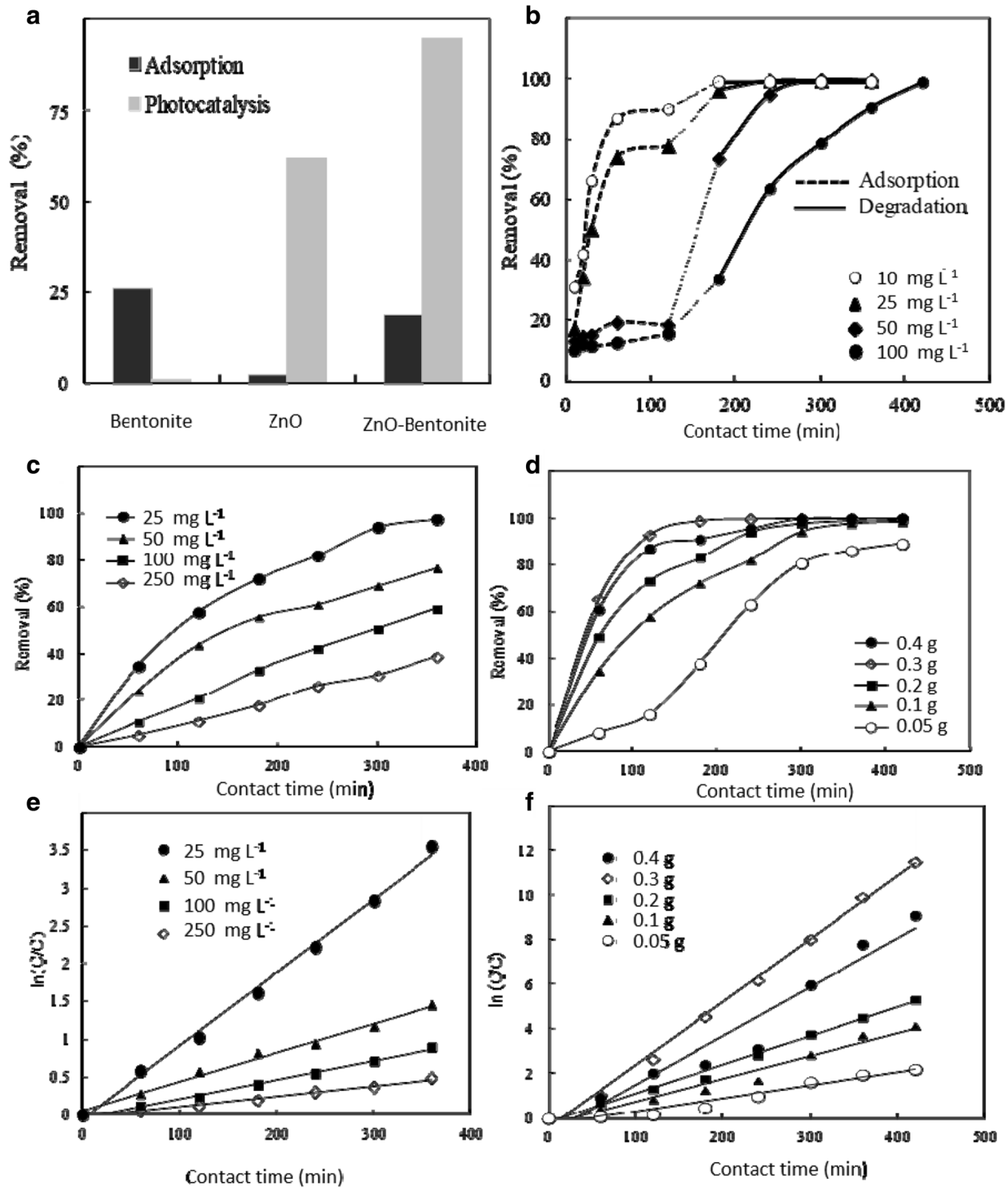

Fig. 3 (**a**) Removal of MB from aqueous solution. Initial MB concentration: 50 mg L^{-1}; Catalyst dose: 2 g L^{-1}, (**b**) Removal of MB by adsorption and photo-catalysis under UV-irradiation with time at different initial concentrations of MB. Thin dotted line is used to differentiate adsorption from photocatalysis. Removal percentage of phenol by photo-decomposition under UV-irradiation with time at (**c**) different initial concentrations, (**d**) different catalyst loading (**e**, **f**) Langmuir-Hinshelwood plots for determination of kinetic rate of photodecomposition, (**e**) different phenol concentrations, and (**f**) different catalyst loading

Synergy between adsorption and photocatalytic degradation of MB

The possible steps for decontamination of water polluted with MB on the Photo-Zn-Bent is proposed on the results obtained from experiment discussed above. The decontamination process probably consists of (i) MB molecules adsorbed onto the surface and (ii) photodegradation of adsorbed MB molecules upon exposure of UV light. Time dependent adsorption and photocatalysis capacities of Photo-Zn-Bent are presented together in Fig. 3b. As shown, MB adsorption has reached equilibrium within 2 h for all investigated concentrations. All experiments consisting of 2 h adsorption and consecutive 2 h photocatalysis reaction were able to fully degrade MB of initial concentration 10 to 25 mg L^{-1}. However, increased initial concentration of MB to 75 and 100 mg L^{-1} required 3–4 h of UV light irradiation, respectively. It can be concluded that the porous structure and high surface area of Bent clay assisted in the photoactivity of ZnO by enhancing adsorption, which is actually the determining step in heterogeneous photocatalysis.

Photocatalytic degradation of phenol

The experiments were repeated with phenol, another potential organic pollutant. As described in the previous experiment, prior to UV illumination, Photo-Zn-Bent was equilibrated with phenol under dark to detect if any adsorption of phenol was taking place. The adsorption of phenol onto Photo-Zn-Bent in all studied concentrations was less than ~10% which was negligible. Hence in all experiments with phenol, initial equilibrium time for adsorption was set as 30 min. Effectiveness of Photo-Zn-Bent for photocatalytic degradation of phenol was tested with different initial concentrations of phenol ranging from 25 to 250 mg L^{-1} as indicated in Fig. 3c and at different catalyst loading ranging from 0.05 to 0.4 g (Fig. 3d). Almost complete degradation of phenol (25 mg L^{-1}) was attained on 6 h of UV-illumination which decreased to ~38% when concentration of phenol increased to 250 mg L^{-1}. Since removal of phenol by Photo-Zn-Bent is completely accounted for photocatalytic reaction, the following 1st-order equation is used to analyse the rate of photocatalytic oxidation [30]:

$$\frac{dC}{dt} = k_{app}C \tag{5}$$

where k_{app} is the apparent rate constant for phenol oxidation.

The influence of initial concentration of the phenol on the degradation rate was calculated using above equation and the results are presented in Table 1 and corresponding Langmuir-Hinshelwood plots are shown in Fig. 3e and f. As shown, the rate decreased with increase of phenol concentration, with a specific dose (2 g L^{-1}) of catalyst. The same trend was proposed by many researchers and the reason was suggested that at high pollutant concentration, all catalytic sites are engaged with no more available sites for pollutant ions to occupy on catalyst surface resulting in decrease of first-order rate constant [33, 34]. In any environmental photocatalysis reactions, the photogeneration of electron-hole pair is followed by the reaction between photo generated hole with hydroxyl radical and organic compounds. According to Gerischer and Heller [34] and Wang et al. [35] when pollutant concentration is high, then the photogeneration of electron-hole pair is the rate governing step. The reaction intermediates may also influence such kinetic behaviour. The photocatalytic oxidation of phenol involves complicated multistage processes. On the surface of excited ZnO particle, phenol molecules were activated by reaction with hydroxyl radicals or positive holes. These oxidizing species are electrophiles that attack electron rich ortho or para positioned carbon atoms. The key intermediates reported were dihydroxybenzene, 4,4′-dihydroxybiphenyl, benzoquinone, and maleic anhydride [36]. These intermediates products, formed in the initial stage, further undergo photocatalytic oxidation, oxidative hydroxylation and decarboxylation to induce ring cleavage to form aliphatic acids such as carboxylic acid and eventually degraded to CO_2 and H_2O [37]. The intermediates may also adsorb onto the catalyst surface through hydrogen bonding, consequently reducing the available active sites for the phenol molecules to be adsorbed. Hence in all our experiments reporting

Table 1 Langmuir-hinshelwood kinetic parameters for photocatalytic removal of phenol as a function of concentration and catalyst loading

Concentration (mg L^{-1})	K_{app} (min^{-1})	R^2
25	1.0×10^{-2}	0.996
50	3.9×10^{-3}	0.990
100	2.5×10^{-3}	0.993
250	1.4×10^{-3}	0.986
Catalyst dose (in 50 mL)		
0.05	5.9×10^{-3}	0.975
0.1	1.0×10^{-2}	0.968
0.2	1.3×10^{-2}	0.992
0.3	2.8×10^{-2}	0.996
0.4	2.2×10^{-2}	0.985

complete decomposition of phenol, UV-illumination is continued until the photodegraded sample solutions show no peak in the entire UV-region, to rule out the possibility of existing any intermediates in the water.

As presented in Fig. 3d, with increase of catalyst loading from 0.5 to 0.1 g, phenol degradation was found rapidly enhanced initially up to an illumination time of 2 h (from 16 to 55% removal of phenol), but with the progress of photoreaction and after 6 h, achieved a degradation of 86 and 99.8% for 0.05 and 0.01 g, respectively. Initial photo oxidation reaction rate increased with increase of catalyst dose from 0.05 to 0.3 g. It may be due to the fact that higher loading of the catalyst provided higher surface area of photoactive sites to adsorb UV light. It is interesting to note that 0.4 g catalyst loading resulted in less photo-decomposition performance than 0.3 g loading. We conclude that high catalyst loading result in blocking of catalyst pores and aggregation thus reducing active surface area. Moreover, the higher catalyst dose would adversely affect UV-light absorption due to increased turbidity. Further it was difficult to maintain the suspension homogeneous and the catalyst settled at the bottom of the reaction vessel, adversely affecting the consistency.

Competitive photocatalytic degradation in organic pollutant mixture

To test the extent of photodegradation efficiency of Photo-Zn-Bent in bicomponent organic pollutant systems, we used phenol and MB (100 mg L^{-1} each) pollutant system. Adsorption experiments for 2 h were conducted prior to each photocatalysis experiments. As shown in Fig. 4a and b, the MB degradation rate remained unaffected in the presence of phenol but the kinetic rate constant of phenol decreased from 9.4×10^{-3} to 1.2×10^{-3} min^{-1} (Table 2). This shows that in a solution containing more than one type of organic contaminants, they compete with each other for the catalyst sites and also with the reaction intermediates. The interaction of organic contaminants with the intermediates should also take into consideration [33]. In this study, the reduction of phenol degradation constant is possibly because of the competition between phenol and MB for the fixed number of

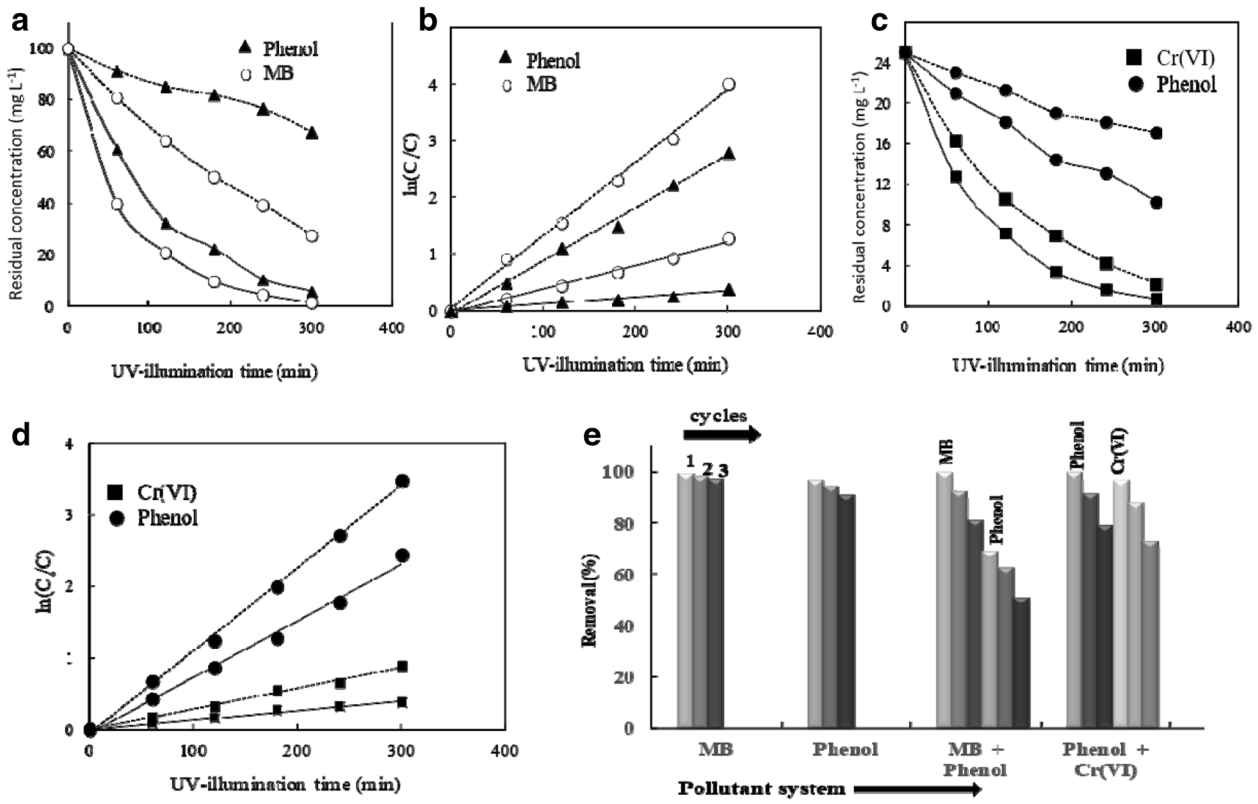

Fig. 4 (**a**, **c**) Variation of residual concentration with time and (**b**, **d**) corresponding Langmuir-Hinshelwood plot for photocatalytic oxidation between (**a**, **b**) phenol and MB (**c**, **d**) phenol and Cr(VI) by Photo-Zn-Bent. Dotted line represents a bi-component photocatalytic system and solid line presents single component system. (**e**) Repeated use of Photo-Zn-Bent for pollutant removal from consecutive three cycles from both single component (MB, Phenol) and bicomponent (MB-Phenol and Phenol-Cr(VI)) pollutant systems

Table 2 The pseudo-first-order rate constants of competitive oxidation of phenol and MB by Photo-Zn-Bent hybrid in single and binary component system

System	Component	Concentration ($mg\ L^{-1}$)	Dose ($g\ L^{-1}$)	k_{app} (min^{-1})	R^2
Binary (Phenol + MB)	Phenol	100	2	1.2×10^{-3}	0.994
	MB	100	2	4.2×10^{-3}	0.996
Single component	Phenol	100	2	9.3×10^{-3}	0.974
	MB	100	2	4.2×10^{-3}	0.992

hydroxyl free radicals. The results from above sections which deal with photodegradation of MB and phenol individually evidenced the greater adsorption of MB than phenol onto Photo-Zn-Bent. Hence, we can assume that MB in the pollutant mixture, due to its higher affinity for the Photo-Zn-Bent surface, is adsorbed more on the catalyst surface. This results in higher degradation by consuming major amount of hydroxyl free radicals generated upon photo illumination. In other words, water containing more than one organic pollutant significantly affects the catalytic activity of the catalyst: the catalyst experiences competition from the pollutant for fixed number of hydroxyl radicals, hence the degradation rate decreases from that of individual rate in a single component system. Moreover, among the competing pollutants, the one with higher affinity for the catalyst surface is degraded more, while inhibiting the degradation of other components.

Synergistic effect on the photocatalytic oxidation of phenol in presence of heavy metal

Further we tested the organic-inorganic binary pollutant system considering synergistic effect in photocatalysis due to co-existence of organic matter and metal ions. It had been reported earlier that the inclusion of organic donors as hole scavengers can accelerate metal reduction, while at the same time declining in its own degradation; the synergy being dependent on the nature of the reducing agent.

Fig. 4c and d shows the degradation profiles of phenol in the absence and presence of Cr(VI). Dilution of the phenol and Cr(VI) in the mixture is adjusted such that both components have same concentration ($25\ mg\ L^{-1}$). It is clear that the presence of Cr(VI) has in fact helped to increase the photodegradation of phenol. The kinetic constant for phenol degradation has increased from 7.9×10^{-3} to 1.2×10^{-2} with Cr(VI) (Table 3). Cr(VI) acted as electron captures and inhibited the recombination, at the same time was reduced to non-toxic Cr(III). It is interesting to note that the extent of Cr(VI) reduction also increased from 1.3×10^{-3} to 2.9×10^{-3} as a result of phenol addition. AAS analysis of the samples indicated same value for the total Cr ion concentration before and after the photocatalytic experiments. Comparing both results obtained from AAS and UV-Vis spectrophotometric analysis, the reduction of Cr(VI) to non-toxic Cr(III) is evident on samples in contact with Photo-Zn-Bent after UV light illumination. The improvement in phenol degradation rate established that Cr(VI) is a competent scavenger of photogenerated electrons. Any significant change in the concentration (from UV-Vis spectrophotometric analysis) of Cr(VI) and phenol was not observed without photocatalyst.

Photo-Zn-bent in repeated adsorption/photocatalysis cycles with different effluents

Behaviour of Photo-Zn-Bent in different waters and in repeated adsorption/photocatalysis cycles was investigated. Besides MB and phenol single pollutant systems, MB/Phenol and Phenol/Cr(VI) systems were also considered as representative of mixed organics and organic-inorganic bicomponent pollutant systems and the results are presented in Fig. 4e. As shown, Photo-Zn-Bent showed an insignificant variation (< 4%) in single component pollutant systems after third cycle

Table 3 Kinetic parameters of simultaneous oxidation and reduction of phenol and Cr(VI), respectively, by Photo-Zn-Bent hybrid in single and binary component system

System	Component	Concentration ($mg\ L^{-1}$)	Dose ($g\ L^{-1}$)	k_{app} (min^{-1})	R^2
Binary (Cr(VI) + Phenol)	Phenol	25	4	1.2×10^{-2}	0.998
	Cr(VI)	25	4	2.9×10^{-3}	0.996
Single component	Phenol	25	4	7.9×10^{-3}	0.998
	Cr(VI)	25	4	1.3×10^{-3}	0.992

as compared to first cycle, indicating effective regeneration of the catalyst after each cycles of application. But in bi-component systems, the catalytic activity of Photo-Zn-Bent was found to decrease significantly after each cycle. In MB/Phenol systems, the activity was decreased to ~25% for phenol, while comparable activity with that of individual is shown for MB in the first cycle. Photo-Zn-Bent retained about ~80% of the activity for MB removal but for phenol, its activity was decreased to ~49% after third cycle, which can be accounted for the competition offered by MB and its intermediates for the available catalyst sites. However, in MB/Phenol system, the total reduction in activity from first cycle to third cycle was the same (~18%) for both MB and phenol. Considering Phenol/Cr(VI) system, Photo-Zn-Bent showed remarkably high activity (~98%) for both phenol and Cr(VI) in the first cycle. But greater reduction in activity (~26%) was observed for both Phenol and Cr(VI) from first to third cycle, which can be accounted as degradation of catalyst to some extent in each cycle of adsorption/photocatalysis experiments. Generally, in organic-metal pollutant systems, the electron hole pair recombination is retarded effectively and hence greater catalytic elimination of both the pollutants can be achieved in the first cycle. Alternatively, the regeneration of catalyst is inhibited to an extent by consuming all the electrons and holes and hence the catalyst life time is decreased eventually leading to the degradation of the catalyst. Still, it is notable that even after three cycles, Photo-Zn-Bent could fairly eliminate ~74% of phenol and Cr(VI) from Phenol/Cr(VI) and ~80% of MB and ~49% of phenol from Phenol/MB mixed effluent systems (initial concentration 100 mg L^{-1} each), which was greater than many other photocatalyst reported in the literature for complex wastewater. Hence Photo-Zn-Bent can be used as a potential recyclable catalyst for treating different types of complex wastewater.

Conclusions

Effective intercalation of ZnO into optimum swelled modified sodium saturated bentonite clay (Photo-Zn-Bent) synergically combined adsorptive nature of bentonite and photo catalysis nature of ZnO. Phenol and MB solutions of lower concentration (25 mg L^{-1}) were completely degraded on the surface of Photo-Zn-Bent hybrid under 6 and 2 h of UV-light irradiation, respectively. The porous structure and high surface area of Bent assisted in the photoactivity of ZnO by enhancing adsorption, which is the determining step in the heterogeneous photocatalysis. The kinetics of photo-degradation of phenol and MB followed Langmuir-Hinshelwood first-order model. High catalyst loading was found unfavourable to the adsorption/photocatalytic activity of Photo-Zn-Bent. Synergic effect of photooxidation and photoreduction was studied in Cr(VI)/phenol system. Co-existence of Cr(VI) with phenol gave higher photoactivity rate for both components. Cr(VI) acted as electron captures and inhibited the recombination, at the same time was reduced to non-toxic Cr(III). Studies with co-existence of phenol and MB in a single system indicated that the degradation rate of MB increased, while that of phenol decreased due to the effective competition for catalyst active sites by the pollutants and their intermediates. Life time of catalyst was found to decrease with repeated use in mixed pollutant systems. The results from performance evaluation conducted for Photo-Zn-Bent in the present study provided the applicability of catalyst for photo-mediated decontamination of textile effluents which are known to contain approximately seven times much more phenol and metal ions than its maximum allowable value. Also, this study indicated in general that even though a hybrid semiconductor, would decontaminate multi-component wastewater streams more efficiently than in single pollutant systems, its life time will considerably decrease due to the degradation of catalyst sites, if used consecutively in multiple cycles. These types of studies are essential for incorporation of photocatalysts onto real world applications.

Additional file

Additional file 1: Figure S1. Process flow chart for the synthesis of Photo-Zn-Bent hybrid. **Figure S2.** SEM images of ZnO and Photo-Zn-Bent. **Figure S3.** EDS spectra of (a) Bent and (b)Photo-Zn-Bent displaying the elemental analysis. (DOCX 1385 kb)

Acknowledgements

All authors thank Director of NIIST-Trivandrum for providing laboratory facilities. SPS acknowledge Council of Scientific and Industrial Research, Government of India and CSIR-Nehru Science Postdoctoral Research Fellowship.

Publisher's Note

Received: 12 July 2018 Accepted: 26 October 2018
Published online: 19 March 2019

References

1. Thi VHT, Lee BK. Great improvement on tetracycline removal using ZnO rod-activated carbon fiber composite prepared with a facile microwave method. J Hazard Mater. 2017;324:329–39.
2. Makrigianni V, Giannakas A, Deligiannakis Y, Konstantinou I. Adsorption of phenol and methylene blue from aqueous solutions by pyrolytic tire char: equilibrium and kinetic studies. J Environ Chem Eng. 2015;3:574–82.
3. Anirudhan TS, Rijith S, Suchithra PS. Preparation and characterization of iron(III) complex of an amino-functionalized polyacrylamide-grafted lignocellulosics and its application as adsorbent for chromium(VI) removal from aqueous media. J Appl Polym Sci. 2010;115:2069–83.
4. Kiran B, Rani N, Kaushik A. Environmental toxicity: exposure and impact of chromium on cyanobacterial species. J Environ Chem Eng. 2016;4:4137–42.

5. Mella B, Glanert AC, Gutterres M. Removal of chromium from tanning wastewater and its reuse. Process Saf Environ. 2015;95:195–201.
6. Linsha V, Suchithra PS, Mohamed AP, Ananthakumar S. Amine-grafted alumino-siloxane hybrid porous granular media: a potential sol-gel sorbent for treating hazardous Cr(VI) in aqueous environment. Chem Eng J. 2013;220:244–53.
7. Wang YT, Latchaw JL. Anaerobic biodegradability and toxicity of hydrogen peroxide oxidation products of phenols. Res J Water Pollut C. 1990;62:234–8.
8. Anirudhan TS, Suchithra PS, Rijith S. Amine-modified polyacrylamide-bentonite composite for the adsorption of humic acid in aqueous solutions. Colloid Surface A. 2008;326:147–56.
9. Anirudhan TS, Suchithra PS. Heavy metals uptake from aqueous solutions and industrial wastewaters by humic acid-immobilized polymer/bentonite composite: kinetics and equilibrium modeling. Chem Eng J. 2010;156:146–56.
10. Anirudhan TS, Suchithra PS, Radhakrishnan PG. Synthesis and characterization of humic acid immobilized-polymer/bentonite composites and their ability to adsorb basic dyes from aqueous solutions. Appl Clay Sci. 2009;43:336–42.
11. Hajjaji M, Alami A, El Bouadili A. Removal of methylene blue from aqueous solution by fibrous clay minerals. J Hazard Mater. 2006;135:188–92.
12. Xie J, Meng WN, Wu DY, Zhang ZJ, Kong HN. Removal of organic pollutants by surfactant modified zeolite: comparison between ionizable phenolic compounds and non-ionizable organic compounds. J Hazard Mater. 2012;231–2:57–63.
13. Anirudhan TS, Tharun AR, Rijith S, Suchithra PS. Synthesis and characterization of a novel graft copolymer containing carboxyl groups and its application to extract uranium(VI) from aqueous media. J Appl Polym Sci. 2011;122:874–84.
14. Anirudhan TS, Divya L, Bringle CD, Suchithra PS. Removal of copper(II) and zinc(II) from aqueous solutions using a lignocellulosic-based polymeric adsorbent containing amidoxime chelating functional groups. Sep Sci Technol. 2010;45:2383–93.
15. Parida KM, Parija S. Photocatalytic degradation of phenol under solar radiation using microwave irradiated zinc oxide. Sol Energy. 2006;80:1048–54.
16. Kavitha MK, Pillai SC, Gopinath P, John H. Hydrothermal synthesis of ZnO decorated reduced graphene oxide: understanding the mechanism of photocatalysis. J Environ Chem Eng. 2015;3:1194–9.
17. Alaraby M, Annangi B, Hernandez A, Creus A, Marcos R. A comprehensive study of the harmful effects of ZnO nanoparticles using *Drosophila melanogaster* as an *in vivo* model. J Hazard Mater. 2015;296:166–74.
18. Sakallioglu T, Bakirdoven M, Temizel I, Demirel B, Copty NK, Onay TT, et al. Leaching of nano-ZnO in municipal solid waste. J Hazard Mater. 2016;317:319–26.
19. Wu CH, Wu CF, Shr JF, Hsieh CT. Parameter settings on preparation of composite photocatalysts for enhancement of adsorption/photocatalysis hybrid capability. Sep Purif Technol. 2008;61:258–65.
20. Wang SY, Ma JY, Li ZJ, Su HQ, Alkurd NR, Zhou WL, et al. Surface acoustic wave ammonia sensor based on ZnO/SiO_2 composite film. J Hazard Mater. 2015;285:368–74.
21. Batistela VR, Fogaca LZ, Favaro SL, Caetano W, Fernandes-Machado NRC, Hioka N. ZnO supported on zeolites: photocatalyst design, microporosity and properties. Colloid Surface A. 2017;513:20–7.
22. Kabra K, Chaudhary R, Sawhney RL. Treatment of hazardous organic and inorganic compounds through aqueous-phase photocatalysis: a review. Ind Eng Chem Res. 2004;43:7683–96.
23. Fatimah I, Wang SB, Wulandari D. ZnO/montmorillonite for photocatalytic and photochemical degradation of methylene blue. Appl Clay Sci. 2011;53:553–60.
24. Meshram S, Limaye R, Ghodke S, Nigam S, Sonawane S, Chikate R. Continuous flow photocatalytic reactor using ZnO-bentonite nanocomposite for degradation of phenol. Chem Eng J. 2011;172:1008–15.
25. Suchithra PS, Shadiya CP, Mohamed AP, Velusamy P, Ananthakumar S. One-pot microwave mediated growth of heterostructured ZnO@AlSi as a potential dual-function eco-catalyst for treating hazardous pollutants in water resources. Appl Catal B Environ. 2013;130–1:44–53.
26. Suchithra PS, Carleer R, Ananthakumar S, Yperman J. A hybridization approach to efficient TiO_2 photodegradation of aqueous benzalkonium chloride. J Hazard Mater. 2015;293:122–30.
27. Meulenkamp EA. Synthesis and growth of ZnO nanoparticles. J Phys Chem B. 1998;102:5566–72.
28. Anirudhan TS, Suchithra PS. Humic acid-immobilized polymer/bentonite composite as an adsorbent for the removal of copper(II) ions from aqueous solutions and electroplating industry wastewater. J Ind Eng Chem. 2010;16:130–9.
29. Lin DD, Pan W, Wu H. Morphological control of centimeter long aluminum-doped zinc oxide nanofibers prepared by electrospinning. J Am Ceram Soc. 2007;90:71–6.
30. Wang YF, Zhang JH, Chen XL, Li X, Sun ZQ, Zhang K, et al. Morphology-controlled fabrication of polygonal ZnO nanobowls templated from spherical polymeric nanowell arrays. J Colloid Interf Sci. 2008;322:327–32.
31. Morales AE, Mora ES, Pal U. Use of diffuse reflectance spectroscopy for optical characterization of un-supported nanostructures. Revista Mexicana de Física S. 2007;53:18–22.
32. Kubelka P, Munk F. An article on optics of paint layers. Z Tech Phys. 1931;12:593–603.
33. Chen DW, Ray AK. Photocatalytic kinetics of phenol and its derivatives over UV irradiated TiO_2. Appl Catal B Environ. 1999;23:143–57.
34. Gerischer H, Heller A. The role of oxygen in photooxidation of organic molecules on semiconductor particles. J Phys Chem US. 1991;95:5261–7.
35. Wang CM, Heller A, Gerischer H. Palladium catalysis of O_2 reduction by electrons accumulated on TiO_2 particles during photoassisted oxidation of organic compounds. J Am Chem Soc. 1992;114:5230–4.
36. Williams MF, Fonfe B, Sievers C, Abraham A, van Bokhoven JA, Jentys A, et al. Hydrogenation of tetralin on silica-alumina-supported Pt catalysts I. Physicochemical characterization of the catalytic materials. J Catal. 2007;251:485–96.
37. Sobczynski A, Duczmal L, Zmudzinski W. Phenol destruction by photocatalysis on TiO_2: an attempt to solve the reaction mechanism. J Mol Catal A Chem. 2004;213:225–30.